Mineralium Deposita (2024) 59:275–290
https://doi.org/10.1007/s00126-023-01202-x

ARTICLE

# Neodymium isotope variations in the Flatreef on Macalacaskop, northern limb, Bushveld Complex

J. J. Keet[1] · F. Roelofse[1] · C. D. K. Gauert[1] · L. M. Iaccheri[2] · D. F. Grobler[3] · H. Ueckermann[4]

Received: 8 June 2022 / Accepted: 9 August 2023 / Published online: 14 September 2023


## Abstract

The origin of the recently discovered Flatreef remains debated due to the pronounced interaction of the magmatic rocks with sedimentary floor rocks, resulting in a complex intrusive stratigraphy. In this study, we report new Nd isotopic compositions of Flatreef lithologies intersected by borehole UMT-393 on the farm Macalacaskop in order to improve our understanding of the magmatic history of the deposit and to further test the putative correlation between the Flatreef/Platreef and the Upper Critical Zone of the remainder of the Bushveld Complex. The initial epsilon Nd ($\varepsilon_{Ndi}$) values for the Flatreef range between −5.2 and −7.6, overlapping with $\varepsilon_{Ndi}$ values of the Upper Critical Zone from the eastern (ranging between −4.8 and −8.5) and the Upper Critical Zone and Main Zone from the western limb (−6.3 and −7.6, and −6.3 and −7.4 respectively) of the Bushveld Complex. The Flatreef $\varepsilon_{Ndi}$ values also overlap with those of the Platreef; however, due to the varying footwall lithologies of the Platreef along strike, Platreef rocks display a wider variation in isotopic composition. Our findings support the correlation of the Flatreef with the Upper Critical Zone — Main Zone transition interval in the remainder of the Bushveld Complex, which includes the Merensky and Bastard reefs. Due to significant overlap between the $\varepsilon_{Ndi}$ values of the Flatreef and local potential contaminants occurring at the base of the Northern Limb, we propose that the Sr–Nd isotopic composition of the magmas that gave rise to the Flatreef are most likely attributable to the interaction of mantle-derived magma with upper and lower crustal rocks of the Kaapvaal Craton within a sub-Bushveld staging chamber, with possible syn- to post-emplacement modification as a result of interaction with dolomitic footwall rocks.

**Keywords** Bushveld complex · Platreef · Flatreef · Nd isotopes · Merensky Reef · Bastard Reef

## Introduction

The Bushveld Complex (BC) (Fig. 1a) is regarded as the most valuable mineral province on Earth (Naldrett 2009). Covering an area of approximately 90,000 km$^2$ (Eales and Cawthorn 1996; Finn et al. 2015), it hosts the world's largest deposits of platinum group elements (PGE), chromium, and vanadium. The Platreef has been suggested to be the equivalent of the Upper Critical Zone in the northern limb of the BC (Grobler et al. 2019). Relative to the Merensky Reef and UG-2 Reef in the western and eastern limbs of the BC, the Platreef in the northern limb has historically attracted less attention from researchers. The Platreef is defined as "Mafic units enriched in Ni-Cu-PGE that occur between the Archaean granite-gneiss basement or the Transvaal Supergroup and the gabbros and gabbronorites of the Main zone, north of the Planknek Fault" (Kinnaird and McDonald 2005, p. B196). Although it is generally accepted that the stratiform mineralization of the upper Platreef is magmatic in

Editorial handling: W. D. Maier

✉ J. J. Keet
beukesj@ufs.ac.za

[1] Department of Geology, University of the Free State, PO Box 339, Bloemfontein 9300, South Africa

[2] Wits Isotope Geoscience Laboratory (WIGL), University of the Witwatersrand, 1 Jan Smuts Avenue, Johannesburg 2000, South Africa

[3] Exploration and Geology, Stillwater Critical Minerals, 904-409 Granville St., Vancouver, Canada

[4] Department of Geology, University of Johannesburg, Auckland Park, P.O. Box 524, Johannesburg 2006, South Africa

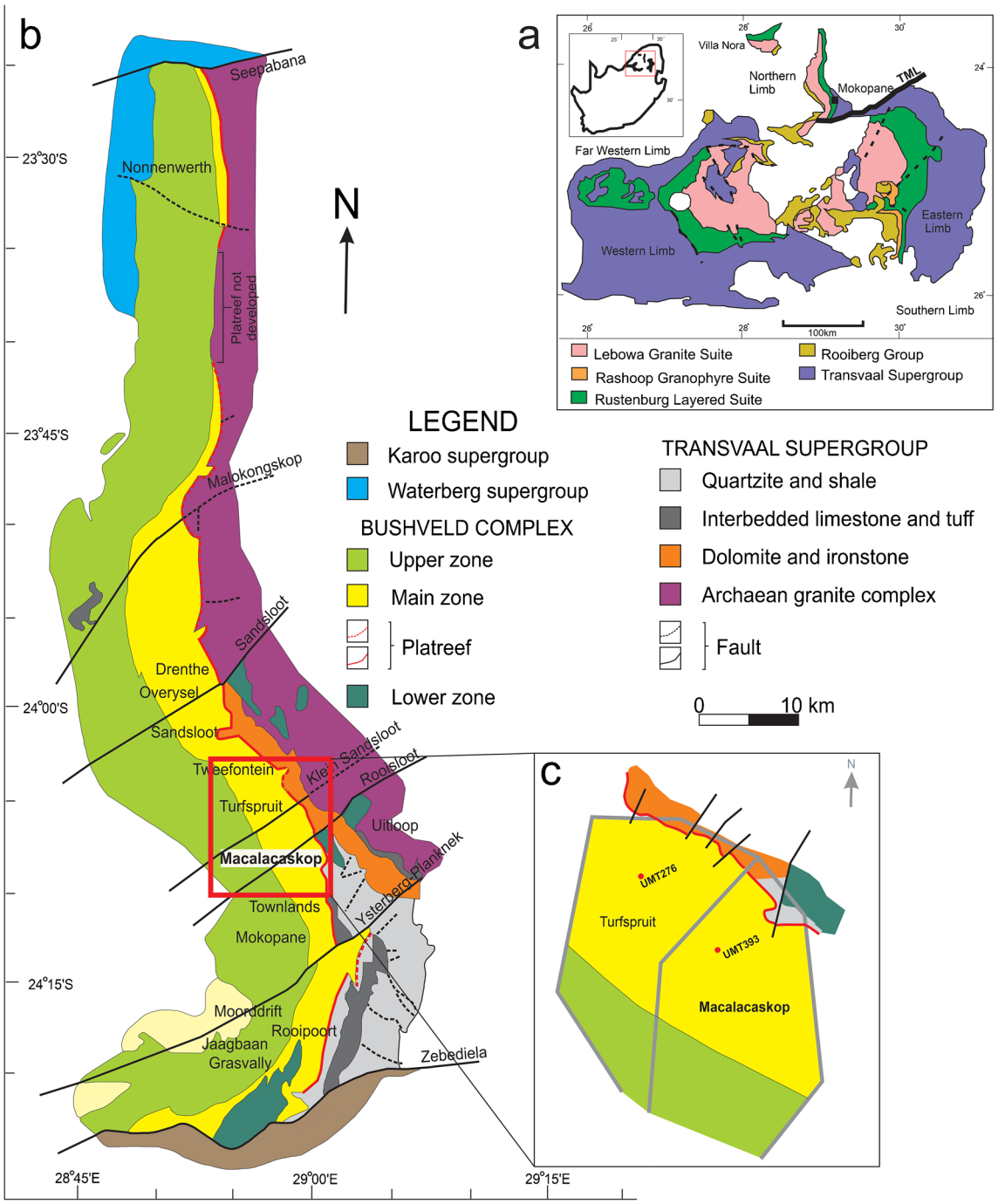


**Fig. 1** **a** Regional map of the BC displaying the different limbs and simplified geology modified after Eales and Cawthorn (1996) and Yudovskaya and Kinnaird (2010). TML = Thabazimbi-Murchison Lineament. **b** Simplified geological map of the northern limb of the BC showing the locations of boreholes UMT-276 and UMT-393 on the farms Turfspruit and Macalacaskop. (After van der Merwe 1976, as modified by Ashwal et al. 2005). **c** An enlarged view of the study area indicating the location of borehole UMT-393

origin (Holwell et al. 2007; Maier et al. 2008; Penniston-Dorland et al. 2008; Yudovskaya et al. 2017; Junge et al. 2019; Klemd et al. 2020), no consensus has been established regarding how the Platreef formed and how it relates to the rest of the BC. Some authors have proposed that the Platreef was emplaced as a sill or multiple sills (Kinnaird 2005; Manyeruke et al. 2005). In contrast, Kruger (2005) suggested that the Platreef formed in response to the intrusion of Main Zone magma that interacted with local floor rocks and subsequently flowed south into the western and

eastern limbs, where it gave rise to the Merensky Reef. Naldrett et al. (2008) proposed a "nested pudding bowls" model where the Platreef formed from PGE-enriched Upper Critical Zone magmas that escaped up the margins between two nested basins.

Isotopic studies have strongly influenced the models for emplacement and petrogenesis of the BC. Early whole-rock Sr-isotopic studies including those of Hamilton (1977), Kruger and Marsh (1982), Sharpe (1985), Lee and Butcher (1990), and Kruger (1994), attributed variations in initial Sr-isotopic composition across the stratigraphy to the repeated intrusion of compositionally distinct magmas. Maier et al. (2000) presented the first whole-rock Nd isotopic data for the Rustenburg Layered Suite. The data were interpreted to reflect the interaction of mantle-derived melt with upper and lower crustal end members. Harris et al. (2005) attributed $\delta^{18}O$ values higher than the mantle range to crustal contamination of parental magmas to the BC within a deep "staging chamber". Extensive crustal contamination of the Bushveld magmas is also supported by S isotopes (Buchanan et al. 1981; Buchanan and Rouse 1984). Various isotopic investigations (O isotopes by Harris and Chaumba (2001), Harris et al. (2005); Os isotopes by Reisberg et al. (2011); Nd isotopes by Pronost et al. (2008), Maier et al. (2008); S isotopes by Buchanan et al. (1981), Manyeruke et al. (2005), Sharman-Harris et al. (2005); Sr isotopes by Cawthorn et al. (1985), Barton et al. (1986), Kruger (2005)) carried out on the Platreef confirm that crustal contamination, in many instances of a localized nature, played a significant role in its formation..

The Flatreef in the northern limb of the BC has led to a better understanding of the provenance and emplacement of the Platreef. The Flatreef is a sub-horizontal, high grade Ni-Cu-PGE orebody, forming a down-dip extension of the Platreef (Grobler et al. 2019). The Flatreef was intersected by Ivanplats (Pty) Ltd. during a deep drilling campaign in 2007. Its stratigraphy is less disturbed and less contaminated than that of the Platreef as the Flatreef does not occur in direct contact with country rocks but commonly overlies thick ultramafic units correlated with the Lower Zone and Lower Critical Zone (Grobler et al. 2019). Beukes et al. (2021) and Mayer et al. (2021) reported the first in situ Sr isotopic data of plagioclase in profiles of the Flatreef as intersected on the farms Macalacaskop and Turfspruit, respectively. Their data are consistent with the Flatreef being a correlate of the Upper Critical Zone — Main Zone transition, as proposed by Grobler et al. (2019). S isotope studies on the Flatreef have shown that the $\delta^{34}S$ values of the main mineralized interval overlap with that of the Merensky Reef in the remainder of the BC (Keir-Sage et al. 2021; Keet et al. 2021). Relatively higher $\delta^{34}S$ values in the lower part of the Flatreef were attributed to crustal assimilation of footwall lithologies. Abernethy (2020), however, reported $\varepsilon_{Ndi}$ values for the Flatreef ranging between −7.2 and −9.2, which are lower than those of the Upper Critical Zone in the Western Bushveld Complex (Maier et al. 2000).

Neodymium isotope ratios are not strongly influenced by syn- or post-magmatic alteration, because Sm–Nd is relatively less mobile in fluids and have comparable geochemical behavior (Rollinson 1993). The complementary Rb–Sr and Sm–Nd isotope systems can be effective tracers of crustal contamination. Compared to Rb–Sr studies, few Nd isotopic studies have been conducted on Bushveld rocks, restricted to the western (Maier et al. 2000; Prevec et al. 2005), eastern (Raines 2014; Bourdeau et al. 2022), and northern limbs (Pronost et al. 2008; Roelofse and Ashwal 2012; Mwenze 2019; Scoon et al. 2020; Abernethy 2020). In this contribution, we present whole-rock Nd-isotopic data on 14 samples across the Flatreef as intersected by drillhole UMT-393 on the farm Macalacaskop. The aim is to further assess the putative correlation between the Flatreef and the Upper Critical Zone, including the Merensky Reef, as known from the rest of the BC.

## The Rustenburg Layered Suite of the northern limb

The BC was emplaced into Transvaal Supergroup sedimentary rocks at ca. 2.055 Ga (Zeh et al. 2015; Scoates et al. 2021) and is formally divided into three plutonic igneous suites, the Rashoop Granophyre Suite, the Lebowa Granite Suite and the mafic–ultramafic Rustenburg Layered Suite (RLS, South African Committee on Stratigraphy 1980) (Fig. 1a).

The RLS crops out in four limbs, namely the eastern, western, far western and northern, and is generally subdivided into 5 stratigraphic zones: the Upper Zone, Main Zone, Critical Zone, Lower Zone, and Marginal Zone (Cawthorn 2015). The northern limb extends for about 110 km from the Zebediela Fault south of Mokopane to the Melinda Fault in the north (Kinnaird et al. 2005) (Fig. 1b).

The stratigraphy of the RLS in the northern limb has been documented by Kinnaird et al. (2005), Ashwal et al. (2005), Yudovskaya et al. (2013), Grobler et al. (2019), and Maier et al. (2021a), and will be briefly summarized here.

## Marginal Zone

The Marginal Zone (MZN) is located at the base of the RLS and comprises of noritic to gabbroic rocks with thicknesses ranging between centimeters to tens of meters (van der Merwe 1976). Rocks forming the lowermost parts of the Platreef were previously incorrectly identified as belonging to the Lower Zone (Maier et al. 2021a).

### Lower Zone

On the farm Turfspruit, the Lower Zone (LZ) is thicker than 700 m, and its lithologies comprise mainly pyroxenite, dunite, and harzburgite (Grobler et al. 2019), whereas on the farm Grasvally, it is up to 1500 m thick comprising of harzburgite, pyroxenite, and chromitite layers (Hulbert and von Gruenewaldt 1982). The presence of these chromitite layers constitute major differences to the LZ in the rest of the BC.

### Critical Zone

In the eastern and western limbs of the BC, the Critical Zone (CZ) is subdivided into 2 zones, the Lower Critical Zone (LCZ) and Upper Critical Zone (UCZ). The LCZ consists predominantly of pyroxenite with minor olivine-bearing units and chromitite layers (Cawthorn 2015). The LCZ was initially believed to be absent from the northern limb (McDonald and Holwell 2011). However, packages of thick ultramafic rocks discovered below the Platreef have subsequently been correlated with the LZ and LCZ (Yudovskaya et al. 2013; Grobler et al. 2019). The Platreef is located at a similar stratigraphic position as the UCZ in the remainder of the BC, below the Main Zone.

### Platreef

The term "Platreef" was coined by van der Merwe (1976) in keeping with the term "Platinum Horizon", used by Wagner (1929), to describe the PGE mineralized basal part of the RLS occurring along the base of much of the northern limb. The Platreef mainly consists of pyroxenite, gabbronorite, norite, peridotite, serpentinite, and a variety of hybrid lithological units, termed parapyroxenite, which formed as a result of significant country rock interaction (McDonald and Holwell 2011). Kinnaird and McDonald (2005) defined the Platreef as Ni-Cu-PGE enriched mafic units positioned between underlying Transvaal Supergroup metasedimentary rocks or Archaean basement granite and overlying Main Zone gabbronorite of the northern limb. However, Maier et al. (2021a) identified various problems with this definition as well as those suggested by other workers (Gain and Mostert 1982; Maier et al. 2008). Preferring the term "Platreef Unit" (Scoon et al 2020), Maier et al. (2021a) defines this unit as a complex sill-like magmatic sequence with metasedimentary xenoliths representing a contaminated analogue of the Upper Critical Zone — Main Zone transition of the western and eastern BC.

The Platreef is generally divided into northern, central and southern sectors on the basis of varying footwall compositions (Merensky 1925; Kinnaird et al. 2005). The southern sector extends from the farms Townlands to Tweefontein where footwall lithologies include shale, banded ironstone, calc-silicate rocks, mudstone, and siltstone of the Duitschland Formation (Fig. 1). The farms Zwartfontein, Sandsloot, Vaalkop, and Tweefontein comprise the central sector and are characterized mainly by dolomitic footwall rocks of the Malmani Subgroup. The northern and far northern sectors extend from Overysel to the Waterberg project and are underlain by granite gneiss. (Kinnaird and Nex 2015). Several large xenoliths of country rock (up to 1.5 km long and 100 m thick) are present in the Platreef (Kinnaird et al. 2005) (Fig. 2). These xenoliths generally have compositions similar to those of the immediate footwall country rocks (Holwell et al. 2007). Where xenolith compositions differ to that of the underlying footwall, it has been suggested that they were transported northwards during emplacement (Holwell et al. 2007).

Relative to the sulfide-poor mineralization of the Merensky Reef and UG-2, the Platreef is thicker and more sulfide-rich (Yudovskaya and Kinnaird 2010). This has stirred debate about the correlation of the Platreef with the UCZ in the remainder of the BC. Some studies (van der Merwe 1976; Kruger 2005) proposed that the interaction of Main Zone magmas with the country rocks resulted in the formation of the Platreef along the footwall contact. However, other studies, such as that of White (1994), suggested that the Platreef may be correlated with the UCZ. New geochemical and isotopic data on the Platreef, including work conducted on the recently discovered Flatreef, support the stratigraphic equivalence between the Platreef/Flatreef and the UCZ inclusive of the Merensky Reef (Grobler et al. 2019; Beukes et al. 2021; Keet et al. 2021; Keir-Sage et al. 2021; Maier et al. 2021b; Mayer et al. 2021).

### Flatreef

The Flatreef is defined as the down-dip extension of the Platreef where laterally continuous, sub-horizontal, PGE mineralized magmatic cyclic units are developed beneath the base of the Main Zone of the northern limb (Grobler et al. 2019). The Flatreef magmatic stratigraphy underlies the farms Turfspruit and Macalacaskop north of Mokopane and is less contaminated and disturbed relative to the shallow Platreef up-dip (Grobler et al. 2019).

The Flatreef stratigraphy is illustrated in Figs. 3 and 4. Grobler et al. (2019) sub-divided the Flatreef into different stratigraphic units, namely, the hanging wall units (HW2 and HW1) which represent the transition zone between the Flatreef and Main Zone, the Bastard Reef, Middling unit, Merensky Reef, and the Footwall Cyclic Unit (FCU). In the present work, the mineralized Merensky Reef and Bastard Reef of the Flatreef will be referred to as the Main Reef and Upper Reef, respectively, in keeping with Yudovskaya et al. (2017). The HW2 unit is the topmost unit of the Flatreef, which consists of mottled

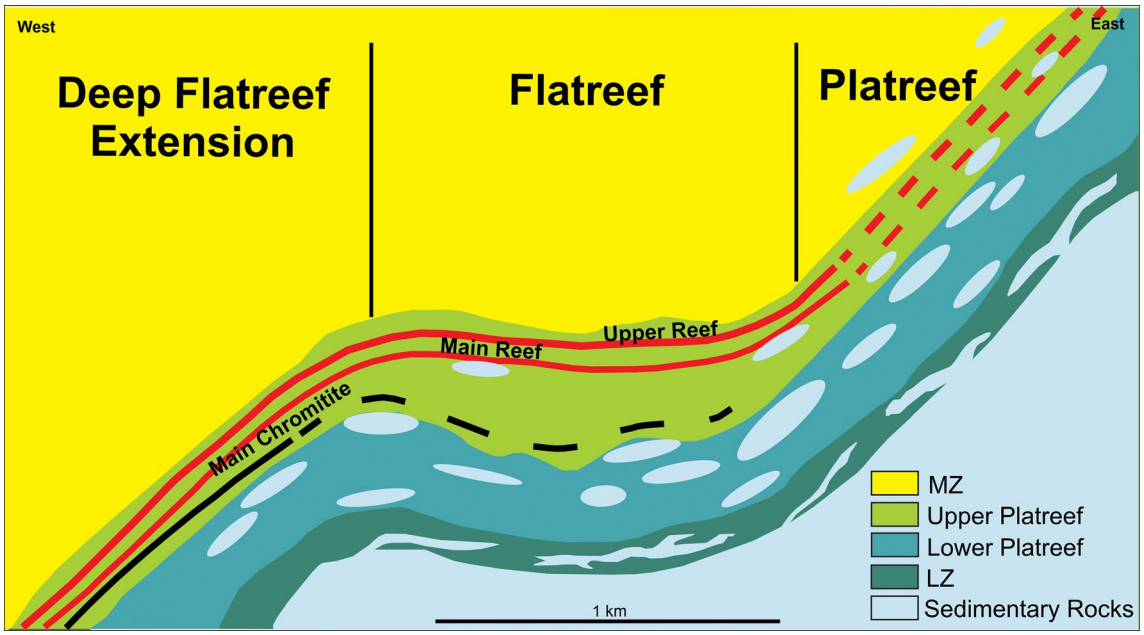


**Fig. 2** Schematic representation of the association between Platreef, Flatreef and the deep Flatreef extension at Turfspruit. Large sedimentary xenoliths are metamorphosed and assimilated by intruding Bushveld magma. Modified after Grobler et al. (2019)

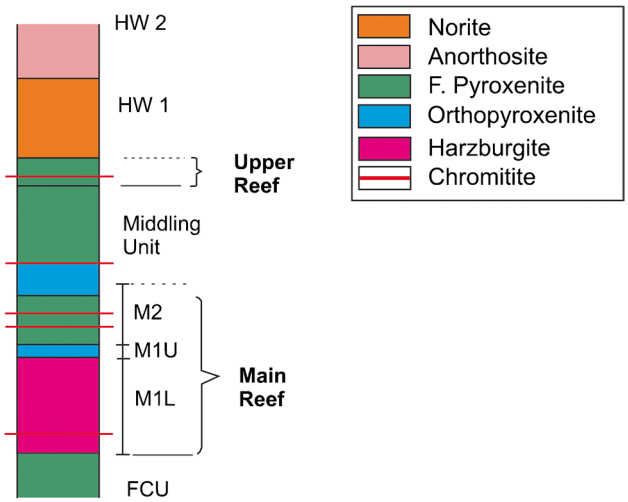


**Fig. 3** Simplified stratigraphic column of the Flatreef in borehole UMT-393, Macalacaskop. Modified after Beukes et al. 2021

anorthosite with an average thickness of 4.2 m. The unit hosts sporadic ultramafic autoliths. The HW1 unit consists of mela- and leucogabbronorite cycles less than 20 m thick. In some drillhole intersections, weakly mineralized interlayered pyroxenite, norite, mottled anorthosite and gabbro are present in the hanging wall unit. The Upper Reef, which is correlated to the Bastard Reef in the western and eastern limbs of the BC, is a pyroxenite between 5 and 10 m thick, with mineralization generally associated with its poorly developed bottom chromitite stringer. Below the Upper Reef is a pyroxenite-norite-anorthosite cyclic unit or feldspathic orthopyroxenite which forms the Middling unit (Md), varying in thickness from a few meters up to 100 m. This unit overlies the Main Reef, a mineralized mafic–ultramafic unit, subdivided into an upper- (M2), and lower portion (M1), which is correlated to the Merensky Reef. The M2 consists of sulfide-rich orthopyroxenite approximately 2 to 10 m thick, bound by an irregular top-, and a more continuous basal chromitite stringer. It is underlain by the M1, which consists of pegmatoidal orthopyroxenite (M1U) and/or pegmatoidal harzburgite (M1L). The FCU underlies the Main Reef and differs along strike in the study area. It consists dominantly of pyroxenite-norite-anorthosite cyclic units.

The presence of country rock xenoliths is common towards the bottom of the Flatreef in close proximity to the floor rocks of the Transvaal Supergroup (Fig. 2).

## Main Zone

The Main Zone (MZ) in the northern limb has a maximum thickness of 2200 m and consists mainly of gabbronorite and norite (van der Merwe 1976). A prominent ultramafic marker layer towards the top of the MZ in the Western Bushveld Complex (WBC) and Eastern Bushveld Complex (EBC), termed the Pyroxenite Marker, is poorly developed or absent in the northern limb (Ashwal et al. 2005; Cawthorn 2020). The occurrence of

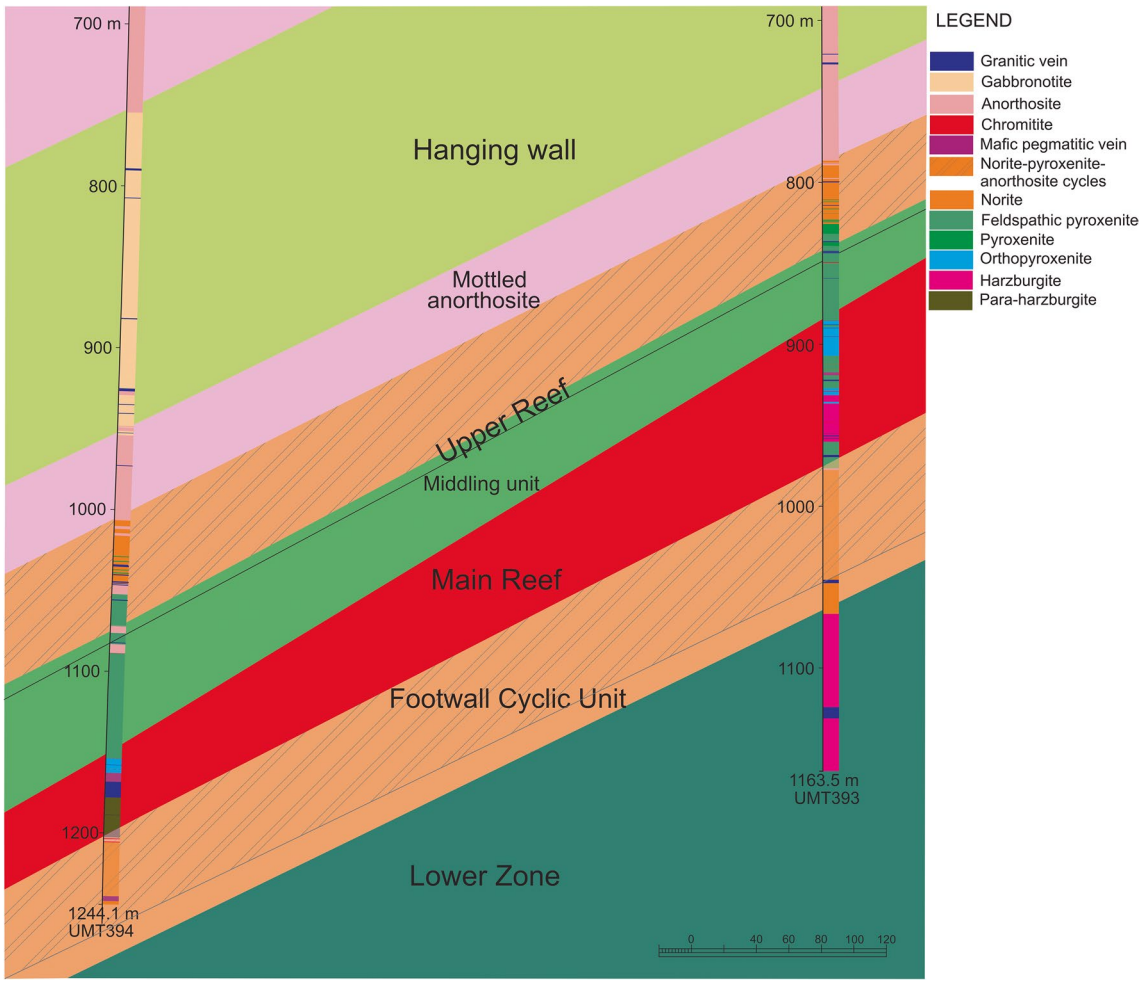


**Fig. 4** Dip section showing the various stratigraphic units of the Flatreef overlying LZ as intersected by borehole UMT-393 and UMT-394. Modified after Keet et al. (2021)

finger-like MZ gabbronorite intrusions into the Platreef at Zwartfontein South pit indicates that emplacement of the MZ postdates formation of the Platreef (Holwell and Jordaan 2006).

### Upper Zone

In the northern limb the Upper Zone (UZ) is ~ 1100 m thick, consisting of gabbro, magnetite gabbro, anorthosite, magnetitite, and olivine diorite (van der Merwe 1976). A total of 32 magnetitite layers were identified in the UZ (Ashwal et al. 2005). The Main Magnetite Layer occurring near the base of the UZ represents the largest vanadium resource on Earth (Cawthorn and Molyneux 1986).

## Location of samples analyzed

Samples of this study were derived from drill core UMT-393 on the farm Macalacaskop (24.122856°S 28.975577°E), and include samples from the HW, Upper Reef, Md unit, Main Reef (M2 and M1) and FCU (Figs. 1c and 3). Borehole UMT-393 is 1163.50 m deep, and intersected 742.63 m of MZ gabbronorite followed by the Flatreef. At Macalacaskop, the footwall consists of quartzite and hornfelsed shale of the Timeball Hill Formation, whereas on the adjacent farm, Turfspruit, the footwall consists of sulfidic shale and limestone of the Duitschland Formation. In the Platreef south of Sandsloot, Transvaal Supergroup metasedimentary rocks separate the Platreef from the underlying LZ

(Yudovskaya et al. 2017). In the UMT-393 intersection at Macalacaskop, the FCU is directly underlain by LZ lithologies (Fig. 4). Here, the FCU consists of interlayered pyroxenite-norite-anorthosite with a total thickness of approximately 98 m. The distribution of base metal sulfides (BMS) in this unit is irregular. Contacts between the interlayered lithologies range from sharp, to undulating to gradational. Minor hybrid lithological layers are observed in particularly poorly developed cyclic units towards the base of the FCU. Three samples from the uppermost 27 m of the FCU were analyzed and consist of medium-grained feldspathic pyroxenite and norite.

The overlying Main Reef, from which 6 samples were analyzed, has a total thickness of about 74 m. The basal portion of the Main Reef (M1L) (Fig. 3) is dominated by harzburgite and is characterized by intensive serpentinization. A thin chromitite stringer is present at a depth of 934 m, close to the basal contact with the underlying FCU. In the M1L, disseminated sulfides and chromite are commonly encountered. The upper portion of the M1 (M1U) is about 5 m thick and consists mainly of mineralized, medium-grained orthopyroxenite. A poorly-developed chromitite stringer is observed near the top contact with the overlying unit at a depth of 928.39 m. The M2 which is the upper portion of the Main Reef consists of mineralized orthopyroxenite and feldspathic pyroxenite, commonly medium-grained with pegmatoidal patches. The M2 exhibits the highest total Pt + Pd concentrations with a maximum of 5 ppm (Beukes et al. 2021).

The Md unit in UMT-393 is located above the Main Reef and consists of feldspathic pyroxenite containing less BMS than the adjacent units. The Upper Reef in UMT-393 consists of sulfide-rich feldspathic pyroxenite. It is characterized by an increase in PGE concentrations associated with a basal chromitite stringer present at a depth of 849 m. The hanging wall unit (HW1 and HW2), which is the uppermost unit of the Flatreef, hosts lithologies that are somewhat similar to those of the FCU, namely, interlayered pyroxenite-norite-anorthosite. Keet et al. (2021) suggested that the hanging wall lithologies may initially have been continuous with the footwall lithologies and were separated by the intrusion of different pulses of the remainder of the Flatreef. The hanging wall, however, contains little to no hybrid lithologies.

## Analytical methods

Powders of the samples were prepared by crushing and milling using a carbon steel jaw-crusher and swing mill, respectively, at the Department of Geology, University of the Free State. Trace element concentrations were determined at the Earth Lab of the University of the Witwatersrand on a Thermo Scientific iCAP RQ Inductively Coupled Plasma Mass Spectrometer (ICP-MS). The samples (50 mg) were weighed and dissolved in a mixture of HF-$HNO_3$ either via a microwave digester or using the open beaker/hotplate method depending on sample solubility. The dissolved samples were subsequently diluted to 50 ml with 5% $HNO_3$ containing Re and Rh (100 ppb) and In and Bi (50 ppb) as internal standards, the concentrations of which were monitored throughout analysis. The certified reference materials BCR-2 and BHVO-2 (Raczek et al. 2001) were analyzed alongside the samples.

For Sm–Nd isotopic analysis, the samples were prepared at the Wits Isotope Geoscience Laboratory of the University of the Witwatersrand. Approximately 300 mg of sample powder was spiked with $^{149}Sm$–$^{150}Nd$ enriched tracer and dissolved in an HF-$HNO_3$ mixture. Ion-exchange chemistry entailed a two-stage separation. Firstly, the bulk LREE were separated from the matrix using PFA columns with a 2-ml resin bed of BioRad AG 50W-X8, 200–400 mesh. After resin equilibration, the samples were loaded into the column in 1-ml 1.5 M HCl. The matrix was eluted in 1.5 M HCl, whereas the LREE were eluted adding 6 M HCl. Subsequently, Nd and Sm were separated on PFA columns using 1-ml LNSpec resin bed as cation exchange medium, and the samples were loaded into the column in 0.3-ml 0.2 M HCl.

Isotopic measurements were performed on a low resolution mode on a Nu Instruments Plasma II MC-ICP-MS (Nu Instrument, Wrexham) housed at the Analytical Facility of the University of Johannesburg. This MC-ICPMS instrument is equipped with 16 Faraday detectors and 5 ion counters. At the start of each measurement session, the instrument was optimized for sensitivity and stability. Samples and standards were introduced in a 2% $HNO_3$ solution using wet plasma, with a self-aspirating 200 µl/min Glass Expansion MicroMist U-series nebulizer. The nebulizer was coupled with a Peltier cooled quartz Glass Expansion Twister Spray Chamber, at 7 °C. An intensity of 1 V was generally obtained for $^{146}Nd$ on a 500 ppb JNdi-1 standard solution. Nd analyses consisted of one block of 60 cycles, each with a 10-s integration time, and Sm analyses of one block of 20 cycles with an integration time of 10 s each. Using these parameters, an internal precision of $< \pm 0.001\%$ (1SE) on fractionation-corrected $^{143}Nd/^{144}Nd$ ratios were obtained.

Backgrounds for all extracts were measured at a magnet offset of half a mass unit away from the measurement position for 30 s directly before commencement of the measurement and subtracted from the signal. Automatic peak centering was performed prior to each measurement. Washout between samples was carried out with a 2% $HNO_3$ solution, monitoring the signals on mass 150 for Nd (the spike isotope), and mass 149 for Sm extracts to decrease back to background, which was usually achieved in less than 5 min.

Data reduction was performed offline using a customized Microsoft Excel spreadsheet. Instrumental mass bias was

determined based on the $^{146}Nd/^{145}Nd$ values of the spiked Nd extract, using $^{146}Nd/^{145}Nd = 2.0719425$, which is equivalent to $^{146}Nd/^{144}Nd = 0.7219$ (Vance and Thirlwall 2002). This was used to calculate a mass bias exponent according to the exponential law. Interference corrections and spike subtractions were then performed to obtain $^{143}Nd/^{144}Nd$ for the sample. Nd concentrations were determined from the corrected mixture $^{150}Nd/^{144}Nd$ ratio. The Sm mass bias exponent was calculated based on the $^{152}Sm/^{147}Sm$ ratio (using the true value of 1.78307) of the spiked Sm extract, to enable the Sm concentration to be calculated from the corrected mixture $^{149}Sm/^{147}Sm$ ratio.

Analysis of the JNdi standard produced a running average of $^{143}Nd/^{144}Nd = 0.512110 \pm 0.000018$ (n = 36) compared to the accepted values published by Tanaka et al. (2000), $^{143}Nd/^{144}Nd = 0.512115 \pm 0.000007$. Initial Nd isotopic ratios ($^{143}Nd/^{144}Nd_i$), were calculated for an age of 2.06 Ga, using a decay constant of $6.54 \times 10^{-12} y^{-1}$ (Lugmair and Marti 1978). The $\varepsilon_{Ndi}$ values were calculated using the present-day composition of CHUR, $^{143}Nd/^{144}Nd = 0.512630$ and $^{147}Sm/^{144}Nd = 0.1960$ (Bouvier et al. 2008).

## Results

Whole-rock trace elements are reported in Electronic Supplementary Materials (ESM) 1, with selected data presented in Table 1. Chondrite-normalized rare earth element patterns of the Flatreef lithologies are similar to those of the UCZ of the Western Bushveld Complex (WBC) as presented by Maier et al. (2013) (Fig. 5). These units appear to be slightly more enriched in LREE compared to HREE. The highest $La_N$ is observed for the HW norite. The REE patterns of the feldspathic pyroxenite of the Flatreef are generally similar with the exception of the HW and M2 sample, hosting a chromitite stringer, where negative Eu anomalies are observed. A similar trend is observed for M1L harzburgite. The Eu anomaly (Eu/Eu*) values for these samples are 0.64, 0.62, and 0.76, respectively (Table 1). The remainder of the analyzed samples display varyingly positive Eu/Eu* values with an average of 1.37 with strong positive Eu/Eu* values observed for HW norite (1.41) and FCU norite (2.65). The Flatreef samples show a lower LREE enrichment ($Ce/Sm_N = 1.89$) relative to that of the UCZ of the WBC ($Ce/Sm_N = 2.89$, Maier et al. 2013). The $Tb/Yb_N$ has an average value of 1 indicating almost no fractionation of HREE.

Nd isotope data are presented in Table 2 and in Fig. 6 where it is shown alongside Sr isotope data from Beukes et al. (2021). The $\varepsilon_{Ndi}$ and $^{87}Sr/^{86}Sr_i$ values were calculated for an age of 2.06 Ga. The $\varepsilon_{Ndi}$ values of the Flatreef units vary between −7.6 and −5.2. The $\varepsilon_{Ndi}$ broadly decreases with increase in stratigraphic height (Fig. 6a). The lowermost analyzed sample of the FCU has an $\varepsilon_{Ndi}$ value of −6.3 followed by −5.4 towards the top. The lower Main Reef has slightly lower $\varepsilon_{Ndi}$ with values ranging between −7.3 and −6.7, whereas the upper Main Reef (M2) has $\varepsilon_{Ndi}$ of between −7.0 and −6.0. The lowest value is located in the Md unit and overlying Upper Reef feldspathic pyroxenite, exhibiting $\varepsilon_{Ndi}$ values of −7.6 and −7.5, respectively. The highest value was recorded for the HW norite with an $\varepsilon_{Ndi}$ value of -5.2. Variations in the average $^{87}Sr/^{86}Sr_i$ ratio for analyzed samples across the Flatreef are presented in Fig. 6b. A general increase in $^{87}Sr/^{86}Sr_i$ with increase in stratigraphic height is observed, with

**Table 1** Selected trace elements and REE (ppm)

| Sample | Depth (m) | Rock type | Strat | V | Cr | Ni | Rb | Sr | Y | Zr | Th | La | Ce | Yb | Eu/Eu* | $(Ce/Sm)_N$ | $(Tb/Yb)_N$ |
|---|---|---|---|---|---|---|---|---|---|---|---|---|---|---|---|---|---|
| JDJ076 | 802.43 | N | HW | 84 | 967 | 227 | 6 | 196 | 4 | 17 | 0.78 | 4.42 | 8.46 | 0.50 | 1.41 | 2.64 | 1.03 |
| JDJ086 | 824.42 | FPX | HW | 134 | 1956 | 447 | 6 | 53 | 6 | 18 | 0.72 | 2.78 | 5.64 | 0.81 | 0.64 | 1.82 | 0.80 |
| JDJ097 | 848.63 | FPX | UR | 127 | 4182 | 1905 | 3 | 59 | 4 | 6 | 0.16 | 2.12 | 3.66 | 0.55 | 1.22 | 2.15 | 0.65 |
| JDJ107 | 877.07 | FPX | Md | 124 | 2091 | 702 | 2 | 58 | 5 | 5 | 0.10 | 2.14 | 4.12 | 0.66 | 1.05 | 1.83 | 0.72 |
| JDJ109A | 884.50 | FPX | Md | 114 | 2001 | 2843 | 7 | 56 | 4 | 5 | 0.08 | 1.51 | 2.54 | 0.57 | 1.37 | 1.98 | 0.55 |
| JDJ112B | 888.98 | FPX | M2 | 103 | 2310 | 1049 | 6 | 90 | 3 | 8 | 0.32 | 1.81 | 3.44 | 0.40 | 1.33 | 2.14 | 0.72 |
| JDJ119 | 912.27 | FPX | M2 | 188 | 3633 | 1160 | 2 | 24 | 6 | 6 | 0.06 | 1.17 | 2.65 | 0.98 | 0.62 | 0.97 | 0.66 |
| JDJ120 | 915.35 | FPX | M2 | 109 | 3676 | 1629 | 5 | 78 | 3 | 4 | 0.08 | 1.29 | 2.42 | 0.43 | 1.33 | 2.00 | 0.57 |
| JDJ126 | 928.39 | OPX | M1U | 122 | 3039 | 585 | 4 | 85 | 5 | 7 | 0.10 | 2.33 | 4.40 | 0.68 | 1.20 | 1.73 | 0.79 |
| JDJ133 | 942.27 | HA | M1L | 95 | 3611 | 2304 | 5 | 26 | 4 | 7 | 0.14 | 1.27 | 2.72 | 0.50 | 0.76 | 1.45 | 0.75 |
| JDJ141A | 960.06 | FPX | M1L | 98 | 3611 | 767 | 2 | 46 | 3 | 5 | 0.05 | 1.08 | 1.84 | 0.54 | 0.99 | 1.34 | 0.59 |
| JDJ152 | 981.20 | FPX | FCU | 112 | 2239 | 490 | 2 | 83 | 3 | 6 | 0.20 | 1.44 | 2.67 | 0.36 | 1.17 | 2.03 | 0.68 |
| JDJ154A | 983.20 | N | FCU | 115 | 2271 | 475 | 2 | 73 | 2 | 5 | 0.12 | 1.23 | 2.00 | 0.34 | 1.32 | 2.00 | 0.56 |
| JDJ163 | 1003.34 | N | FCU | 107 | 854 | 133 | 3 | 248 | 3 | 9 | 0.25 | 2.58 | 4.64 | 0.31 | 2.65 | 2.32 | 1.00 |

*N, FPX, OPX, and HA indicate norite, feldspathic pyroxenite, orthopyroxenite, and harzburgite, respectively

*HW, UR, Md, M1U, M1L, and FCU indicate hanging wall, Upper Reef, Middling unit, M1 Upper, M1 Lower, and the Footwall Cyclic unit, respectively

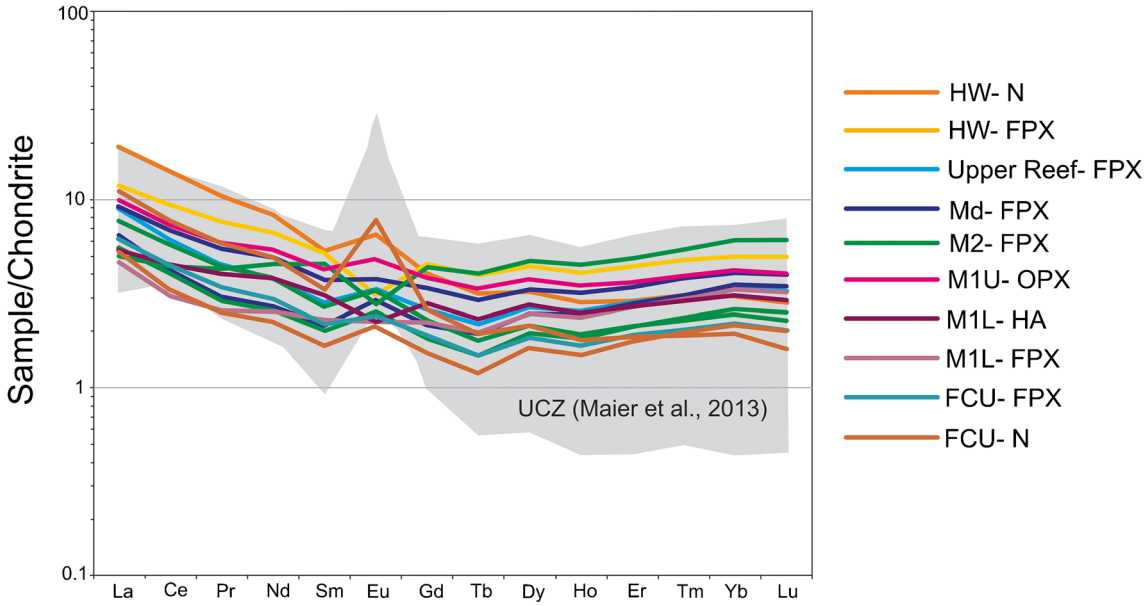


**Fig. 5** Chondrite-normalized REE plot of the Flatreef samples (Table 1, ESM Table 1). The area in grey represents data of the UCZ (excluding UG-2) as reported by Maier et al. (2013). Normalizing values are taken from Anders and Grevesse (1989). HW, UR, Md, M1U, M1L, and FCU indicate hanging wall, Upper Reef, Middling unit, M1 Upper, M1 Lower and the Footwall Cyclic unit, respectively. N, FPX, OPX and HA indicate norite, feldspathic pyroxenite, orthopyroxenite and harzburgite, respectively

**Table 2** $\varepsilon_{Ndi}$ data calculated for an age of 2.06 Ga

| Sample | Depth (m) | Rock type | Unit | Nd (ppm) | Sm (ppm) | $^{147}Sm/^{144}Nd$ | $^{143}Nd/^{144}Nd$ (measured) | $\varepsilon_{Ndi}$ | 2SE |
|---|---|---|---|---|---|---|---|---|---|
| JDJ076 | 802.43 | N | HW | 4.07 | 0.84 | 0.1241 | 0.511388 | −5.24 | 0.55 |
| JDJ086 | 824.42 | FPX | HW | 3.23 | 0.81 | 0.1521 | 0.511717 | −6.21 | 0.53 |
| JDJ097 | 848.63 | FPX | UR | 1.89 | 0.47 | 0.1488 | 0.511605 | −7.53 | 0.54 |
| JDJ107 | 877.07 | FPX | Md | 2.33 | 0.58 | 0.1497 | 0.511631 | −7.26 | 0.53 |
| JDJ109A | 884.50 | FPX | Md | 1.36 | 0.36 | 0.1589 | 0.511740 | −7.58 | 0.58 |
| JDJ112B | 888.98 | FPX | M2 | 1.84 | 0.43 | 0.1411 | 0.511564 | −6.32 | 0.54 |
| JDJ119 | 912.27 | FPX | M2 | 2.25 | 0.73 | 0.1954 | 0.512267 | −6.96 | 0.55 |
| JDJ120 | 915.35 | FPX | M2 | 1.27 | 0.32 | 0.1526 | 0.511735 | −6.00 | 0.61 |
| JDJ126 | 928.39 | OPX | M1U | 2.66 | 0.69 | 0.1567 | 0.511731 | −7.18 | 0.52 |
| JDJ133 | 942.27 | HA | M1L | 1.95 | 0.52 | 0.1609 | 0.511815 | −6.65 | 0.57 |
| JDJ141A | 960.06 | FPX | M1L | 1.20 | 0.35 | 0.1765 | 0.511993 | −7.30 | 0.62 |
| JDJ152 | 981.20 | FPX | FCU | 1.54 | 0.37 | 0.1441 | 0.511653 | −5.36 | 0.57 |
| JDJ154A | 983.20 | N | FCU | 1.14 | 0.28 | 0.1510 | 0.511736 | −5.56 | 0.58 |
| JDJ163 | 1003.34 | N | FCU | 2.46 | 0.54 | 0.1337 | 0.511466 | −6.26 | 0.57 |

*N, FPX, OPX, and HA indicate norite, feldspathic pyroxenite, orthopyroxenite, and harzburgite, respectively

*HW, UR, Md, M1U, M1L, and FCU indicate hanging wall, Upper Reef, Middling unit, M1 Upper, M1 Lower, and the Footwall Cyclic unit, respectively

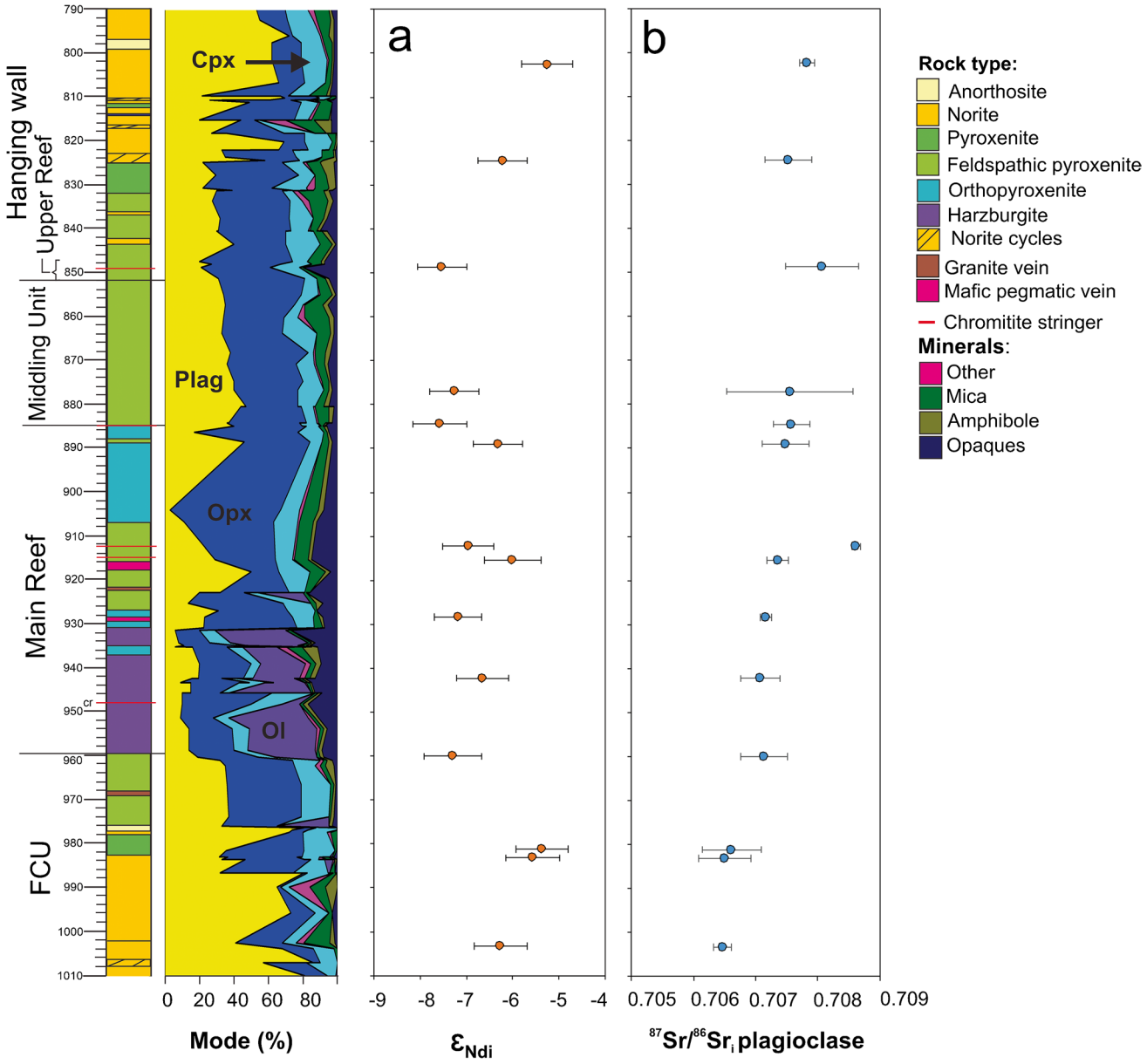


**Fig. 6** Variation in mineral modes, $\varepsilon_{Ndi}$, and $^{87}Sr/^{86}Sr_i$ with increase in stratigraphic height across Flatreef stratigraphy as intersected by borehole UMT-393. Error bars represent 2SE and 2σ for $\varepsilon_{Ndi}$ and $^{87}Sr/^{86}Sr_i$, respectively. The Sr data are from Beukes et al. (2021). Epsilon Nd and initial Sr values are calculated for an age of 2.06 Ga

a pronounced increase in the upper portion of the Main Reef. The Nd and Sr isotope compositions are therefore inversely proportional as shown by the weak negative correlation between $\varepsilon_{Ndi}$ and $^{87}Sr/^{86}Sr_i$ in Fig. 7a. These data overlap with UCZ anorthosite/norite/pyroxenite and MZ gabbronorite data of the WBC (Fig. 7a). Similarly, Th/La ratios plotted against $^{87}Sr/^{86}Sr_i$ and $\varepsilon_{Ndi}$, respectively (Fig. 7b and c) overlap with WBC data, displaying a weak negative correlation in Fig. 7b, and no clear correlation is distinguishable in Fig. 7c.

## Discussion

### Comparison between Platreef/Flatreef and Rustenburg Layered Suite of the remainder of the Bushveld Complex

Previous studies have shown a range of Nd isotopic values from across the BC (Fig. 8). For the UCZ of the western limb, $\varepsilon_{Ndi}$ values vary between − 6.3 and − 7.6, and for the

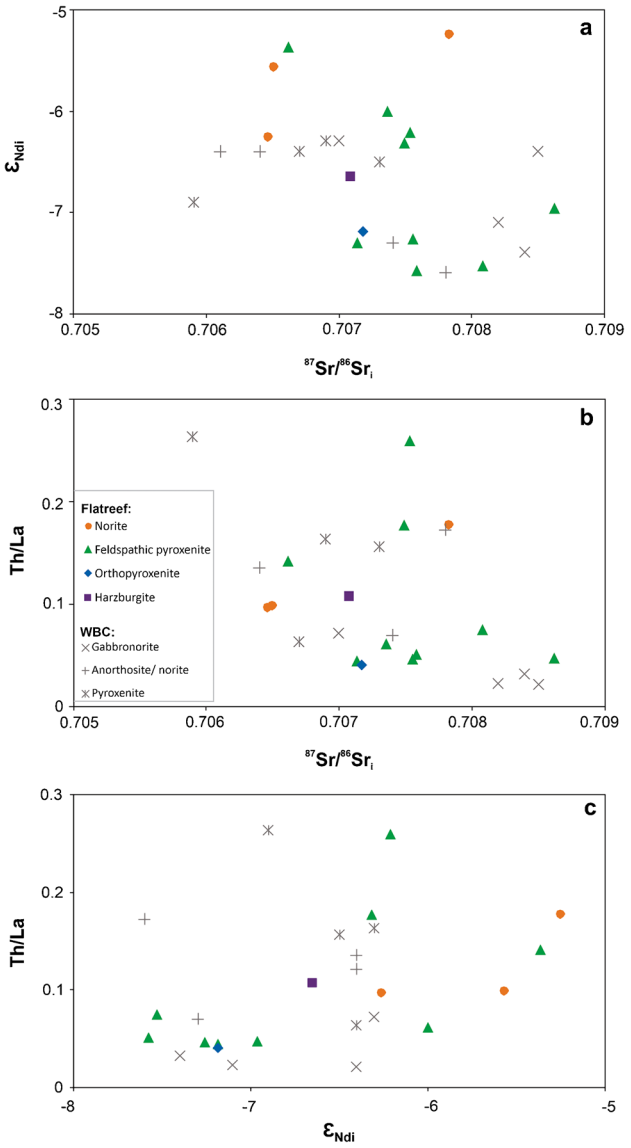


**Fig. 7** Binary variation diagrams of **a** $\varepsilon_{Ndi}$ vs $^{87}Sr/^{86}Sr_i$, **b** Th/La vs $^{87}Sr/^{86}Sr_i$, and **c** Th/La vs $\varepsilon_{Ndi}$ in Flatreef rocks. WBC data from Maier et al. (2000) are included for comparison (grey symbols). The Sr data are from Beukes et al. (2021). Epsilon Nd and initial Sr values are calculated for an age of 2.06 Ga

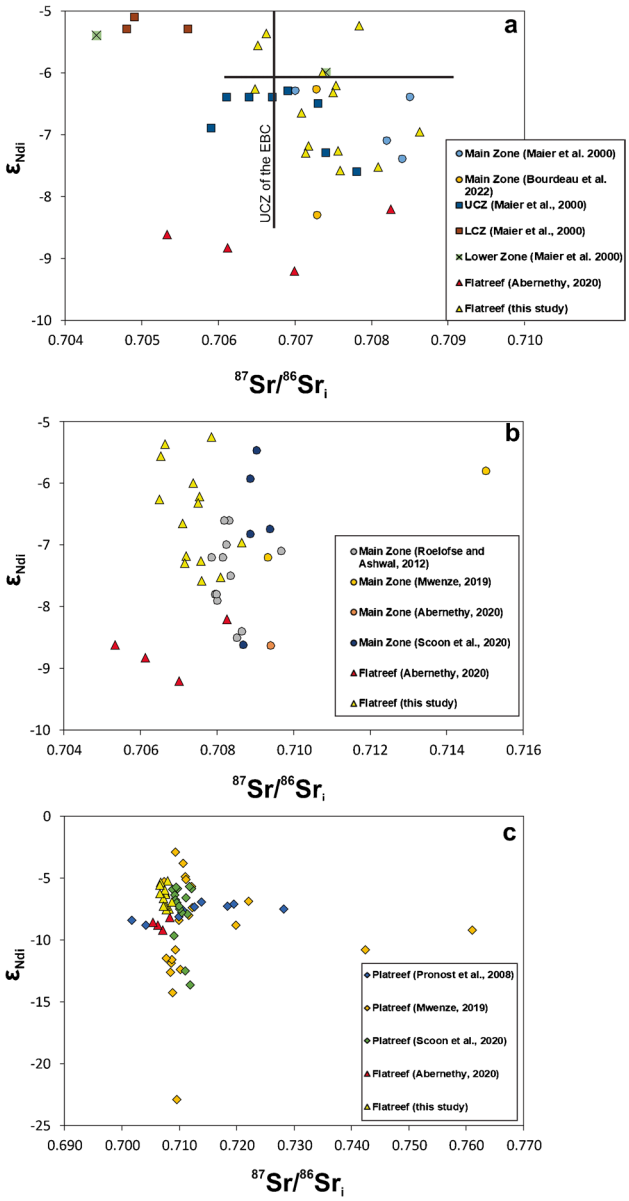


**Fig. 8** Plot of $\varepsilon_{Ndi}$ vs $^{87}Sr/^{86}Sr_i$ for the **a** Flatreef (Abernethy 2020; this study, Sr data are from Beukes et al. (2021)), samples of the Rustenburg Layered Suite of the western limb (Maier et al. 2000) and eastern limb (Lee and Butcher 1990; Raines 2014; Bourdeau et al. 2022) of the Bushveld Complex; **b** Flatreef samples (Table 2) and adjacent farm, Turfspruit (Abernethy 2020) and Main Zone samples (Roelofse and Ashwal 2012; Mwenze 2019; Abernethy 2020; Scoon et al. 2020) of the northern limb; **c** Flatreef samples (Table 2; Abernethy 2020) and Platreef samples (Pronost et al. 2008; Mwenze 2019; Scoon et al. 2020) of the northern limb

MZ between – 6.3 and – 7.4 (Maier et al. 2000). The $\varepsilon_{Ndi}$ values reported for the Merensky Reef interval at Winnaarshoek range from – 8.5 to – 4.5 (Raines 2014). Boudreau et al. (2022) analyzed two MZ samples from the Apel anorthosite sequence in the eastern limb, an anorthosite and gabbronorite, having $\varepsilon_{Ndi}$ of – 8.3 and – 6.3, respectively. Previous Sr and Nd isotopic work on the MZ of the northern limb showed $\varepsilon_{Ndi}$ ranging between – 8.6 and – 6.6 and $^{87}Sr/^{86}Sr_i$ ranging between 0.708 and 0.715 (Roelofse and Ashwal 2012; Mwenze 2019; Abernethy 2020; Scoon et al. 2020).

The Platreef rocks display a wide variety of isotopic compositions (Fig. 8). Pronost et al. (2008) reported $\varepsilon_{Ndi}$ values for Platreef rocks in the northern limb at the farms Sandsloot, where floor rock comprises dolomite from the Transvaal Supergroup, and Overysel, underlain by Archaean granite footwall rocks, ranging from – 7.0 to – 7.3 and – 8.8 to – 7.1, respectively. $^{87}Sr/^{86}Sr_i$ varies between 0.711 and 0.718 at Sandsloot, and 0.701 and 0.728 at Overysel.

However, a broader variation in isotopic composition was reported by Mwenze (2019) for Sandsloot ($\varepsilon_{Ndi}$ − 22.9 to − 2.9, $^{87}Sr/^{86}Sr_i$ 0.708 to 0.710), Overysel ($\varepsilon_{Ndi}$ − 10.8 to − 4.9, $^{87}Sr/^{86}Sr_i$ 0.708 to 0.742) and Tweefontein, which is underlain by Transvaal Supergroup BIF and shale ($\varepsilon_{Ndi}$ − 14.3 to − 5.1, $^{87}Sr/^{86}Sr_i$ 0.707 to 0.760). At Akanani (near Sandsloot, Fig. 1b), where Platreef rocks are underlain by Transvaal dolomite floor rocks, $\varepsilon_{Ndi}$ varies between − 13.7 and 1.3, and $^{87}Sr/^{86}Sr_i$ between 0.709 and 0.712 (Scoon et al. 2020). Although $\varepsilon_{Ndi}$ values reported in this study fall within the same range as that of the Platreef rocks (Fig. 8c), differences are observed in Nd-isotopic composition of the mineralized units. For example, the $\varepsilon_{Ndi}$ values of the Main Mineralized Reef at Akanani are distinctly lower ($\varepsilon_{Ndi}$ average of − 11.4) than our results for the Main Reef ($\varepsilon_{Ndi}$ average of − 6.7). It is possible that the parental magma associated with the Main Mineralized Reef was more severely contaminated with crust. Alternatively, it has been proposed that the Main Mineralised Reef magma may be derived from metasomatized sub-continental lithospheric mantle (Scoon et al. 2020; Wasch et al. 2009). Other Sr isotopic studies on the Platreef have returned $^{87}Sr/^{86}Sr_i$ values ranging from 0.711 to 0.723 and 0.705 to 0.715 at Overysel and Sandsloot, respectively (Barton et al. 1986), and 0.710 to 0.711 at Turfspruit (Kruger 2005).

Beukes et al. (2021), Mayer et al. (2021), and our study show that the Sr and Nd isotope compositions of the Flatreef rocks strongly overlap with that of the Merensky Reef and Bastard Reef in the remainder of the BC. Our findings show that $\varepsilon_{Ndi}$ values across the Flatreef stratigraphy vary between − 5.2 and − 7.6, significantly overlapping with both the UCZ and MZ rocks of the eastern and western limbs of the BC (Raines 2014; Boudreau et al. 2022; Maier et al. 2000) (Fig. 8a). Abernethy (2020) reported $\varepsilon_{Ndi}$ values for the Flatreef on Turfspruit, ranging from − 7.2 to − 9.2. These values are significantly lower than what we report for the Flatreef as well as on the data from the UCZ and MZ (Maier et al. 2000; Raines 2014; Boudreau et al. 2022) in the remainder of the BC. The relatively low values of $\varepsilon_{Ndi}$ from Turfspruit may indicate increased contamination. Abernethy proposed between 23 and 55% with higher estimates for the lower Flatreef. The contaminants used in the mixing models were footwall calcareous sediments (Abernethy 2020), granite (Johannesburg Dome, Barton et al. 1999; banded gneiss from Overysel, Pronost et al. 2008; granite end member, Telus et al. 2012) and shale (Hunter and Hamilton 1978; Beukes et al. 1990; Jahn and Condie 1995 and Li et al. 2010). Sr and Nd isotopes display inverse covariation, hence relative to $^{87}Sr/^{86}Sr_i$, a weak inverse trend is observed when $\varepsilon_{Ndi}$ is plotted against stratigraphic height (Fig. 6). The $\varepsilon_{Ndi}$ decreases through the Main Reef, MD and Upper Reef. Beukes et al. (2021) and Mayer et al. (2021) showed an increase in Sr at the base of the main mineralized interval of the Flatreef from 0.707 to > 0.709 at Macalacaskop and 0.706 to 0.709 at Turfspruit.

## Sr–Nd isotopic constraints on the petrogenesis of the Flatreef

The identification of an isotopic shift at the base of the main mineralized interval of the Flatreef, similar to the isotope shift described for the EBC and WBC (Kruger 1994; Karykowski et al. 2017), is consistent with the suggestion of Grobler et al. (2019) that the Flatreef sequence is a correlate of the Merensky and Bastard Units in the remainder of the BC. Whole-rock $\delta^{34}S$ data across the Flatreef show that the Main Reef has a consistent near-mantle S isotopic signature similar to that of the Merensky Reef in the remainder of the BC, further supporting the contention that the Flatreef is a correlate of the UCZ-MZ transition interval (Keet et al. 2021; Keir-Sage et al. 2021). Our Nd isotope data are also consistent with these findings.

Although the significantly more radiogenic Sr isotope composition of Platreef rocks may be attributed to local floor rock contamination, it is evident that the Nd isotopic composition of the Flatreef cannot be accounted for by the mixing of mantle-derived melt with Transvaal Supergroup rocks (Fig. 9). Our Nd isotope data overlap with that of the Rooiberg Group (Buchanan et al. 2004), Transvaal Supergroup sedimentary rocks (Jahn and Condie 1995; Pronost et al. 2008; Abernethy 2020), Johannesburg Dome tonalite and granite (Barton et al. 1999), Ancient Gneiss Complex (Barton et al. 1980; Carlson et al. 1983), Archaean granite gneiss (Pronost et al. 2008), and Turfloop Batholith (Henderson et al. 2000). One of the mixing models presented in Fig. 10 shows that in order to reproduce the observed Sr–Nd isotopic compositions for the Flatreef would necessitate a mantle-derived melt being contaminated with > > 80% of Transvaal devolatilized carbonate footwall. Thermal and bulk-rock compositional constraints firmly exclude this as a possible petrogenetic model for the Flatreef.

Our preferred model to explain the Sr–Nd isotopic composition of the Flatreef is in keeping with Roelofse and Ashwal (2012), who showed that the isotopic composition of rocks of the RLS can be explained through the interaction of mantle-derived magma with upper and lower crustal lithologies derived from the Kaapvaal Craton within a sub-Bushveld staging chamber. As shown in Fig. 10, the Flatreef has Nd-isotopic compositions similar to a 60:40 B1:B2 mixture proposed by Barnes et al. (2010) to be parental magma to the Merensky Reef of the WBC, but the Flatreef exhibits consistently more radiogenic Sr-isotopic compositions compared to this mixture, with data points falling along a mixing array between a 60:40 B1:B2 mixture and Transvaal devolatilized carbonate footwall. We suggest that the Sr-isotopic

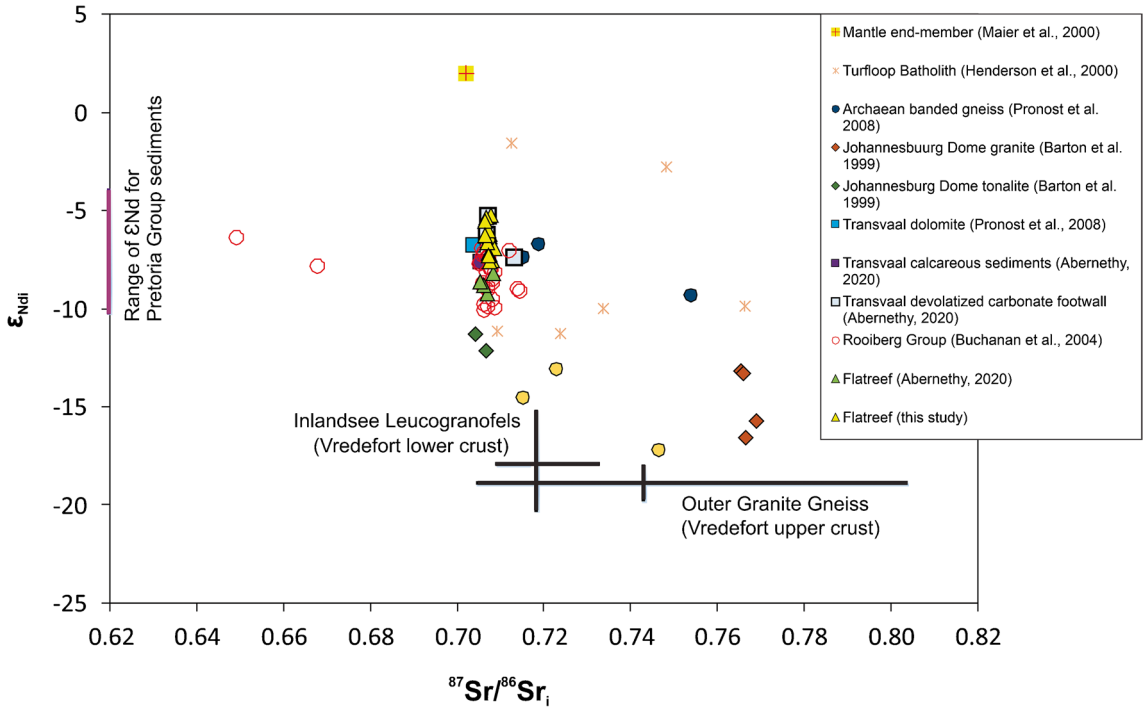


**Fig. 9** Plot of $\varepsilon_{Ndi}$ vs $^{87}Sr/^{86}Sr_i$ calculated at 2.06 Ga of whole-rock data for the Transvaal Supergroup, Turfloop Batholith, Archaean granite gneiss, the Johannesburg Dome, the Rooiberg Group, the Vredefort Dome OGG and ILG, the Flatreef (the Sr data are from Beukes et al. (2021)) and a mantle melt end member ($\varepsilon_{Ndi}=2$, $^{87}Sr/^{86}Sr_i=0.702$, Maier et al. 2000); modified after Roelofse and Ashwal 2012

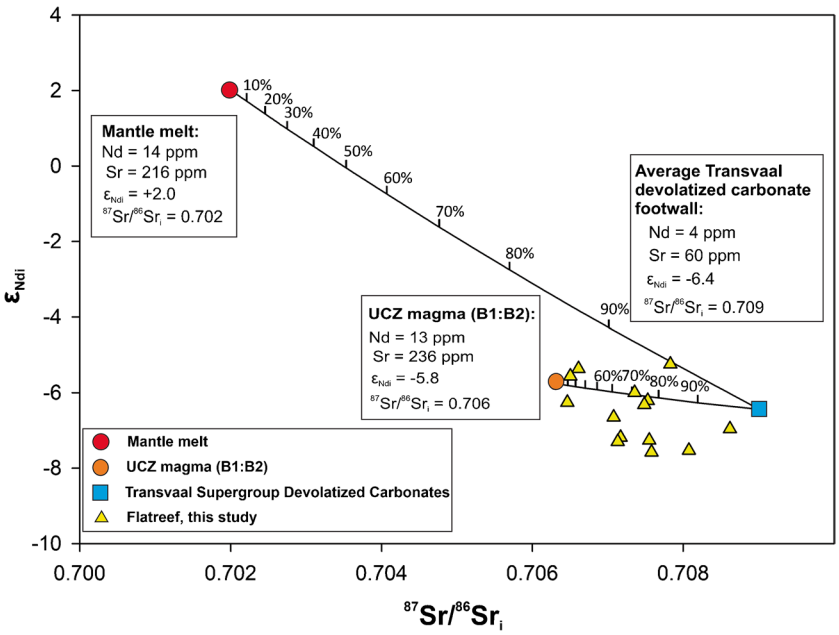


**Fig. 10** Isotopic mixing models for mixtures between mantle-derived melt ($\varepsilon_{Ndi}=2.0$, $^{87}Sr/^{86}Sr=0.702$, Maier et al. 2000; Nd = 14 ppm, Sr = 216 ppm, Roelofse and Ashwal 2012) and a 60:40 B1:B2 mixture ($\varepsilon_{Ndi}=-5.8$, $^{87}Sr/^{86}Sr_i=0.706$, Nd = 13 ppm, Sr = 236 ppm, Curl 2001) respectively, and devolatized Transvaal Supergroup carbonates ($\varepsilon_{Ndi}=-6.4$, $^{87}Sr/^{86}Sr_i=0.709$, Nd = 4 ppm, Sr = 60 ppm, Abernethy 2020)

composition of the Flatreef may have been modified by localized syn- to post-emplacement interaction between UCZ magma and dolomitic footwall rocks of the Transvaal Supergroup.

The HW and FCU lithologies have similar $\varepsilon_{Ndi}$ values (average of − 5.7), both being higher than that of the lithologies in the remainder of the Flatreef. This supports the proposal by Keet et al. (2021), that the main mineralized

Flatreef units intruded into the originally continuous package of the HW and FCU lithologies.

## Conclusions

Our $\varepsilon_{Ndi}$ values display significant overlap with UCZ-MZ data of the WBC and EBC. Our findings are consistent with isotope studies on the Flatreef which provide further support for the proposed correlation of the Flatreef stratigraphy with that of the uppermost UCZ, including the mineralized Merensky and Bastard Reefs (Grobler et al. 2019). The highest $\varepsilon_{Ndi}$ values of the Flatreef are observed in the hanging wall and footwall units which could suggest that that these units were originally continuous but were subsequently separated by magma pulses that formed the mineralized units of the Flatreef. The Nd isotopic composition of the Flatreef cannot be accounted for by the interaction between mantle-derived magma and local contaminants occurring as footwall rocks along the eastern margin of the Northern Limb. Instead, the magma(s) that gave rise to the Flatreef were likely derived from a sub-Bushveld staging chamber in which mantle-derived melts interacted with lower and upper crustal rocks of the Kaapvaal Craton (Roelofse & Ashwal 2012). However, the Flatreef exhibits Sr-isotopic compositions that are consistently more radiogenic than those expected for the mixture of magmas (60:40 B1:B2) that gave rise to the UCZ, a feature that may point to syn- to post-emplacement modification of the isotopic composition of the parental magma through interaction with local dolomitic rocks of the Transvaal Supergroup.

**Supplementary Information** The online version contains supplementary material available at https://doi.org/10.1007/s00126-023-01202-x.

**Acknowledgements** This study was supported by an nGAP grant (UID 119698) to J.J.K. The authors would like to thank Ivanplats for access to the samples analyzed as part of this study, and Marlin Patchappa (EarthLab – University of the Witwatersrand) for geochemical analyses. Thorough reviews by Steve Prevec and an anonymous reviewer , as well as the associate editor, Wolfgang Maier, allowed us to significantly improve the manuscript.

**Funding** Open access funding provided by University of the Free State.

## Declarations

**Conflict of interest** The authors declare no competing interests.



## References

Abernethy K (2020) Geochemistry and petrology of the Flatreef, as exposed in deep drill cores UMT 081 and 94. PhD thesis, Cardiff University, 332pp

Anders E, Grevesse N (1989) Abundances of the elements: meteoritic and solar. Geochimica et Cosmochimica Acta 53:197–214

Ashwal LD, Webb SJ, Knoper MW (2005) Magmatic stratigraphy in the Bushveld Northern Lobe: continuous geophysical and mineralogical data from the 2950m Bellevue drill core. S Afr J Geol 108:199–232

Barnes S-J, Maier WD, Curl EA (2010) Composition of the marginal rocks and sills of the Rustenburg Layered Suite, Bushveld Complex, South Africa: implications for the formation of the platinum-group element deposits. Econ Geol 105:1491–1511

Barton JM, Hunter DR, Jackson MPA, Wilson AC (1980) Rb-Sr age and source of the Bimodal Suite of the Ancient Gneiss Complex, Swaziland. Nature 283:756–758

Barton JM, Cawthorn RG, White J (1986) The role of contamination in the evolution of the Platreef of the Bushveld Complex. Econ Geol 81:1096–1104

Barton JM, Barton ES, Kröner A (1999) Age and isotopic evidence for the origin of the Archaean granitoid intrusives of the Johannesburg Dome, South Africa. J Afr Earth Sci 28:693–702

Beukes NJ, Klein C, Kaufman AJ, Hayes JM (1990) Carbonate petrography, kerogen distribution, and carbon and oxygen isotope variations in an Early Proterozoic transition from the limestone to iron-formation deposition, Transvaal Supergroup, South Africa. Econ Geol 85:663–690

Beukes JJ, Roelofse F, Gauert CDK, Grobler DF, Ueckermann H (2021) Strontium isotope variations in the Flatreef on Macalacaskop, northern limb, Bushveld Complex: implications for the source of platinum-group elements in the Merensky Reef. Miner Deposita 56:45–57

Bourdeau JE, Hayes B, Zhang SE, Logue A, Bybee GM (2022) Origin and significance of noritic blocks in layered anorthosites in the Bushveld Complex, South Africa. Contrib Mineral Petrol 177:1–26

Bouvier A, Vervoort JD, Patchett PJ (2008) The Lu-Hf and Sm-Nd isotopic composition of CHUR: constraints from unequilibrated chondrites and implications for the bulk composition of terrestrial planets. Earth Planet Sci Lett 2073:48–57

Buchanan DL, Rouse JE (1984) Role of contamination in the precipitation of sulphides in the Platreef of the Bushveld Complex. In: Buchanan DL, Jones MJ (eds) Sulphide deposits in mafic and ultramafic rocks. IMM, London, pp 141–146

Buchanan DL, Nolan J, Suddaby P, Rouse JE, Viljoen MJ, Davenport JWJ (1981) The genesis of sulfide mineralization in a portion the Potgietersrus Limb of the Bushveld Complex. Econ Geol 76:568–579

Buchanan PC, Reimold WU, Koeberl C, Kruger FJ (2004) Rb-Sr and Sm-Nd isotopic compositions of the Rooiberg Group, South Africa: early Bushveld-related volcanism. Lithos 29:373–388

Carlson RW, Hunter DR, Barker F (1983) Sm-Nd age and isotopic systematics of the bimodal suite, ancient gneiss complex, Swaziland. Nature 305:701–704

Cawthorn RG (2015) The Bushveld Complex, South Africa. In: Charlier B, Namur O, Latypov R, Tegner C (eds) Layered intrusions. Springer, Netherlands, pp 517–587

Cawthorn RG (2020) Massive pyroxene compositional oscillations on a metre scale in the Pyroxenite Marker, northern limb, Bushveld Complex. South Africa Lithos 356–357:105392
Cawthorn RG, Molyneux TG (1986) Vanadiferous magnetite deposits of the Bushveld Complex. In: Anhaeusser CR, Maske S (eds) Mineral deposits of Southern Africa. Geol Soc S Afr Johannesburg 2:1251–1266
Cawthorn RG, Barton JM, Viljoen MJ (1985) Interaction of floor rocks with the Platreef on Overysel, Potgietersrus, Northern Transvaal. Econ Geol 80:988–1006
Curl EA (2001) Parental magmas of the Bushveld Complex, South Africa. PhD thesis, Monash University, Australia, p 140
Eales HV, Cawthorn RG (1996) The Bushveld Complex. In: Cawthorn RG (ed) Layered intrusions. Elsevier, Oxford, pp 181–229
Finn CA, Bedrosian PA, Cole JC, Khoza TD, Webb SJ (2015) Mapping the 3-D extent of the Northern Lobe of the Bushveld layered mafic intrusion from geophysical data. Precambr Res 268:279–294
Gain SB, Mostert AB (1982) The geological setting of the platinoid and base metal sulfide mineralization in the Platreef of the Bushveld Complex in Drenthe, north of Potgietersrus. Econ Geol 77:1395–1404
Grobler DF, Brits JAN, Maier WD, Crossingham A (2019) Litho- and chemostratigraphy of the Flatreef PGE deposit, northern Bushveld Complex. Miner Deposita 54:3–28
Hamilton PJ (1977) Sr isotope and trace element studies of the Great Dyke and Bushveld mafic phase and their relation to early Proterozoic magma genesis in southern Africa. J Petrol 18:24–52
Harris C, Chaumba JB (2001) Crustal contamination and fluid-rock interaction during the formation of the Platreef, northern limb of the Bushveld Complex, South Africa. J Petrol 42:1321–1347
Harris C, Pronost J, Ashwal LD, Cawthorn RG (2005) Oxygen and hydrogen isotope stratigraphy of the Rustenburg Layered Suite, Bushveld Complex: constraints on crustal contamination. J Petrol 46:579–601
Henderson D, Long L, Barton J Jr (2000) Isotopic ages and chemical and isotopic composition of the Archaean Turfloop Batholith, Pietersburg granite—greenstone terrane, Kaapvaal Craton, South Africa. S Afr J Geol 103:38–46
Holwell DA, Jordaan A (2006) Three-dimensional mapping of the Platreef at the Zwartfontein South mine: Implications for the timing of magmatic events in the northern limb of the Bushveld Complex, South Africa. Trans Inst Min Metall 115:B41–B48
Holwell DA, Boyce AJ, McDonald I (2007) Sulfur isotope variations within the Platreef Ni-Cu-PGE deposit: genetic implications for the origin of sulphide mineralization. Econ Geol 102:1001–1110
Hulbert LJ, Von Gruenewaldt G (1982) Nickel copper and platinum mineralisation in the Lower Zone of the Bushveld Complex, South of Potgietersrus. Econ Geol 77:1296–1306
Hunter DR, Hamilton PJ (1978). In: Tarling DH (ed) The Bushveld Complex. Evolution of the earth's crust. Academic Press, London
Jahn B, Condie KC (1995) Evolution of the Kaapvaal craton as viewed from geochemical and Sm-Nd isotopic analyses of intracratonic pelites. Geochim Cosmochim Acta 59:2239–2258
Junge M, Oberthür T, Kraemer D, Melcher F, Piña R, Derrey IT, Manyeruke T, Strauss H (2019) Distribution of platinum-group elements in pristine and near-surface oxidized Platreef ore and the variation along strike, northern Bushveld Complex, South Africa. Mineral Deposita 54:885–912
Karykowski BT, Yang S-H, Maier WD, Lahaye Y, Lissenberg C, O'Brien H (2017) In situ Sr isotope compositions of plagioclase from a complete stratigraphic profile of the Bushveld Complex, South Africa: evidence for extensive magma mixing and percolation. J Petrol 58:2285–2308
Keet JJ, Roelofse F, Gauert CDK, Grobler D, Butler M (2021) A comparative study of sulfur isotope variations within the Flatreef and Merensky Reef of the Bushveld Complex, South Africa. Can Mineral 59:1363–1380
Keir-Sage E, Leybourne MI, Jugo PJ, Grobler DF, Mayer CC (2021) Assessing the extent of local assimilation within the Flatreef, northern limb of the Bushveld Igneous Complex, using sulfur isotopes and trace element geochemistry. Miner Deposita 56:91–102
Kinnaird JA (2005) Geochemical evidence for multiphase emplacement in the southern Platreef. Appl Earth Sci (Trans. Inst. Min. Metal. lB) 114:B225–242
Kinnaird JA, McDonald I (2005) An introduction to mineralisation in the northern limb of the Bushveld Complex. Appl Earth Sci 114:194–198
Kinnaird JA, Nex PAM (2015) An overview of the Platreef. In: Hammond NQ, Hatton C (eds) Platinum-group element (PGE) mineralisation and resources of the Bushveld Complex, Council for Geoscience, Pretoria, South Africa, pp 293–341
Kinnaird JA, Hutchinson D, Schurmann L, Nex PAM, de Lange R (2005) Petrology and Mineralisation of the southern Platreef: northern limb of the Bushveld Complex, South Africa. Miner Deposita 40:576–597
Klemd R, Beinlich A, Kern M, Junge M, Martin L, Regelous M, Schouwstra R (2020) Magmatic PGE sulphide mineralization in clinopyroxenite from the Platreef, Bushveld Complex, South Africa. Minerals 10(6):570
Kruger FJ (1994) The Sr-isotopic stratigraphy of the western Bushveld Complex. S Afr J Geol 97:393–398
Kruger FJ (2005) Filling the Bushveld Complex magma chamber: lateral expansion, roof and floor interaction, magmatic unconformities, and the formation of giant chromitite, PGE and Ti-V-magnetitite deposits. Miner Deposita 40:451–472
Kruger FJ, Marsh JS (1982) Significance of 87Sr/86Sr ratios in the Merensky cyclic unit of the Bushveld Complex. Nature 298:53–55
Lee CA, Butcher AR (1990) Cyclicity in the Sr isotope stratigraphy through the Merensky reef and Bastard reef units, Atok section, eastern Bushveld Complex. Econ Geol 85:877–883
Li WY, Teng FZ, Ke S, Rudnick RL, Gao S, Wu FY, Chappell BW (2010) Heterogeneous magnesium isotopic composition of the upper continental crust. Geochim Cosmochim Acta 74:6867–6884
Lugmair GW, Marti K (1978) Lunar initial $^{143}Nd/^{144}Nd$: differential evolution line of the lunar crust and mantle. Earth Planet Sci Lett 39:349–357
Maier WD, Arndt NT, Curl EA (2000) Progressive crustal contamination of the Bushveld Complex: evidence from Nd isotopic analyses of the cumulate rocks. Contrib Mineral Petrol 140:316–327
Maier WD, de Klerk L, Blaine J, Manyeruke T, Barnes SJ, Stevens MVA, Mavrogenes JA (2008) Petrogenesis of contact-style PGE mineralization in the northern lobe of the Bushveld Complex: comparison of data from the farms Rooipoort, Townlands, Drenthe and Nonnenwerth. Miner Deposita 43:255–280
Maier WD, Barnes S-J, Groves DI (2013) The Bushveld Complex, South Africa: formation of platinum-palladium, chrome- and vanadium-rich layers via hydrodynamic sorting of a mobilized cumulate slurry in a large, relatively slowly cooling, subsiding magma chamber. Miner Deposita 48:1–56
Maier WD, Jugo P, Yudovskaya M (2021a) Introduction paper to thematic issue on the Flatreef PGE deposit, northern Bushveld Complex. Miner Deposita 56:1–10
Maier WD, Abernethy KEL, Grobler DF, Moorhead G (2021b) Formation of the Flatreef deposit, northern Bushveld, by hydrodynamic and hydromagmatic processes. Miner Deposita 56:11–30
Manyeruke TD, Maier WD, Barnes S-J (2005) Major and trace element geochemistry of the Platreef on the farm Townlands, northern Bushveld Complex. S Afr Geol 108:381–396
Mayer CC, Jugo PJ, Leybourne MI, Grobler DF, Voinot A (2021) Strontium isotope stratigraphy through the Flatreef PGE-Ni-Cu

mineralization at Turfspruit, northern limb of the Bushveld Igneous Complex: evidence of correlation with the Merensky Unit of the eastern and western limbs. Miner Deposita 56:59–72
McDonald I, Holwell DA (2011) Geology of the Northern Bushveld Complex and the setting and genesis of the Platreef Ni-Cu-PGE Deposit. Society of Economic Geologists. Rev Econ Geol 17:297–327
Merensky H (1925) Report on the platinum occurrence on the properties of Potgietersrust Platinums Limited. Report to Shareholders, London and Rhodesia Mining and Land Company Ltd., Johannesburg, South Africa, 6pp
Mwenze T (2019) The implications of Sr and Nd isotope data on the genesis of the Platreef and associated BMS and PGE mineralisation, Bushveld Igneous Complex, South Africa. PhD thesis, University of the Western Cape, 148pp
Naldrett AJ (2009) Fundamentals of magmatic sulfide deposits. In: Li C, Ripley EM (eds) New developments in magmatic Ni–Cu and PGE deposits. Geol Publ House, pp 1–26
Naldrett T, Kinnaird J, Wilson A, Chunnett G (2008) Concentration of PGE in the Earth's crust with special reference to the Bushveld Complex. Earth Sci Front 15:264–297
Penniston-Dorland SC, Wing BA, Nex PAM, Kinnaird JA, Farquhar J, Brown M, Sharman ER (2008) Multiple sulfur isotopes reveal a primary magmatic origin for the Platreef PGE deposit, Bushveld Complex, South Africa. Geology 36:979–982
Prevec SA, Ashwal LD, Mkaza MS (2005) Mineral disequilibrium in the Merensky Reef, western Bushveld Complex, South Africa: new Sm-Nd isotopic evidence. Contrib Miner Petrol 149:306–315
Pronost J, Harris C, Pin C (2008) Relationship between footwall composition, crustal contamination, and fluid-rock interaction in the Platreef, Bushveld Complex, South Africa. Miner Deposita 43:825–848
Raczek I, Stoll B, Hofmann AW, Jochum KP (2001) High precision trace element data for the USGS reference materials BCR-1, BCR-2, BHVO-2, AGV-1, AGV-2, DTS-1, DTS-2, GSP-1and GSP-2 by ID-TIMS and MIC-SSMS. J Geostand Geoanal 25:77–86
Raines MD (2014) An assessment of equilibrium in the Merensky Reef: a textural, geochemical and Nd isotope study of coexisting plagioclase and orthopyroxene from Winnaarshoek in the eastern Bushveld Complex, RSA. MSc dissertation, Rhodes University, 159pp
Reisberg L, Tredoux M, Harris C, Coftier A, Chaumba J (2011) Re and Os distribution and Os isotope composition of the Platreef at the Sandsloot-Mogolakwena mine, Bushveld complex, South Africa. Chem Geol 281:352–363
Roelofse F, Ashwal LD (2012) The Lower Main Zone in the Northern Limb of the Bushveld Complex - a > 1.3 km thick sequence of intruded and variably contaminated crystal mushes. J Petrol 53:1449–1476
Rollinson HR (1993) Using geochemical data: evaluation, presentation, interpretation. Routledge, Harlow
Scoates JS, Wall CJ, Friedman RM, Weis D, Mathez EA, Van Tongeren JA (2021) Dating the Bushveld Complex: timing of crystallization, duration of magmatism, and cooling of the world's largest layered intrusion and related rocks. J Petrol 62:1–39
Scoon RN, Costin G, Mitchell A, Moine B (2020) Non-sequential injection of PGE-rich ultramafic sills in the Platreef unit at Akanani, northern limb of the Bushveld Complex: evidence from Sr and Nd isotopic systematics. J Petrol. https://doi.org/10.1093/petrology/egaa032
Sharman-Harris ER, Kinnaird JA, Harris C, Horstmann UE (2005) A new look at sulphide mineralisation of the northern limb, Bushveld Complex: a stable isotope study. Trans Inst Min Metal Section 114:B252-263
Sharpe MR (1985) Strontium isotope evidence for preserved density stratification in the main zone of the Bushveld Complex, South Africa. Nature 316:119–126
South African Committee for Stratigraphy (SACS) (1980) Kent LE (Compiler) Stratigraphy of South Africa. Geol Surv S Afr Pretoria, Handbook 8:690
Tanaka T, Togashi S, Kamioka H, Amakawa H, Kagami H, Hamamoto T, Yuhara M, Orihashi Y, Yoneda S, Shimizu H et al (2000) JNdi-1: a neodymium isotopic reference in consistency with LaJolla neodymium. Chem Geol 168:279–281
Telus M, Dauphas N, Moynier F, Tissot FLH, Teng FZ, Nabelek PI, Craddock PR, Groat LA (2012) Iron, zinc, magnesium and uranium isotopic fractionation during continental crust differentiation: The tale from migmatites, granitoids, and pegmatites. Geochim Cosmochim Acta 97:247–265
van der Merwe MJ (1976) The layered sequence of the Potgietersrus Limb of the Bushveld Complex. Econ Geol 71:1337–1351
Vance D, Thirlwall M (2002) An assessment of mass discrimination in MC-ICPMS using Nd isotopes. Chem Geol 185:227–240
Wagner P (1929) The platinum deposits and mines of South Africa. Struick, London
Wasch LJ, Van der Zwan FM, Nebel O, Morel MLA, Hellebrand EWG, Pearson DG, Davies GR (2009) An alternative model for silica enrichment in the Kaapvaal subcontinental lithospheric mantle. Geochim Cosmochim Acta 73:6894–6917
White JA (1994) The Potgietersrus prospect – geology and exploration history XVth CMMI Congress, South Africa. South Afr Inst Min Metall 3:173–181
Yudovskaya MA, Kinnaird JA (2010) Chromite in the Platreef (Bushveld Complex, South Africa): occurrence and evolution of its chemical composition. Miner Deposita 45:369–391
Yudovskaya MA, Kinnaird JA, Sobolev AV, Kuzmin DV, McDonald I, Wilson AH (2013) Petrogenesis of the lower zone olivine-rich cumulates beneath the Platreef and their correlation with recognized occurrences in the Bushveld Complex. Econ Geol 108:1923–1952
Yudovskaya MA, Kinnaird JA, Grobler DF, Costin G, Abramova VD, Dunnet T, Barnes S-J (2017) Zonation of Merensky style platinum mineralization in Turfspruit thick reef facies (northern limb of the Bushveld Complex). Econ Geol 112(6):1333–1365
Zeh A, Ovtcharova M, Wilson AH, Schaltegger U (2015) The Bushveld Complex was emplaced and cooled in less than one million years – results of zirconology, and geotectonic implications. Earth Planet Sci Lett 418:103–114